Journal of Molecular Spectroscopy 348 (2018) 130–136

Contents lists available at ScienceDirect

Journal of Molecular Spectroscopy

journal homepage: www.elsevier.com/locate/jms

Remote sensing of methane with OSAS-lidar on the $2\nu_3$ band Q-branch: Experimental proof

Sandrine Galtier [a], Christophe Anselmo [a], Jean-Yves Welschinger [b], J.F. Sivignon [a], Jean-Pierre Cariou [c], Alain Miffre [a], Patrick Rairoux [a,*]

[a] Institut Lumière Matière, CNRS, UMR 5306, Université Lyon 1, 69622 Villeurbanne, France
[b] Institut Camille Jordan, UMR 5208, Université Lyon 1, 69622 Villeurbanne cedex, France
[c] Leosphere France, 14-16 rue Jean Rostand, 91400 Orsay, France

ARTICLE INFO

Article history:
Received 30 September 2017
In revised form 9 February 2018
Accepted 13 February 2018
Available online 14 February 2018

Keywords:
Methane
Absorption spectroscopy
Lambert-Beer-Bouguer
Similitude
Absorption line parameters
Mid infrared
Femtosecond laser
Lidar

ABSTRACT

Optical sensors based on absorption spectroscopy play a central role in the detection and monitoring of atmospheric trace gases. We here present for the first time the experimental demonstration of OSAS-Lidar on the remote sensing of CH_4 in the atmosphere. This new methodology, the OSAS-Lidar, couples the Optical Similitude Absorption Spectroscopy (OSAS) methodology with a light detection and ranging device. It is based on the differential absorption of spectrally integrated signals following Beer Lambert-Bouguer law, which are range-resolved. Its novelty originates from the use of broadband laser spectroscopy and from the mathematical approach used to retrieve the trace gas concentration. We previously applied the OSAS methodology in laboratory on the $2\nu_3$ methane absorption band, centered at the 1665 nm wavelength and demonstrated that the OSAS-methodology is almost independent from atmospheric temperature and pressure. In this paper, we achieve an OSAS-Lidar device capable of observing large concentrations of CH_4 released from a methane source directly into the atmosphere. Comparison with a standard in-situ measurement device shows that the path-integrated concentrations retrieved from OSAS-Lidar methodology exhibit sufficient sensitivity (2 000 ppm m) and observational time resolution (1 s) to remotely sense methane leaks in the atmosphere. The coupling of OSAS-lidar with a wind measurement device opens the way to monitor time-resolved methane flux emissions, which is important in regards to future climate mitigation involving regional reduction of CH_4 flux emissions.

1. Introduction

Climate change in the Earth depends on the change in energy in the atmosphere, the oceans and the continents. Because the atmosphere is the first absorbing interface of this climate system, which is driven by solar energy, its comprehension and characterization is important. It is qualitatively well-known that atmospheric radiative forcing in terms of energy change rate per square meter is affected by the presence of numerous compounds and especially the greenhouses gases H_2O, CO_2, CH_4, N_2O and CFC11-12 accounting for 98% of the atmospheric radiative forcing [1]. This lead, through complex phenomena, to an increase of the mean surface temperature of 0.85° since the end of the 19th century (1880). The quantitative and precise evaluation of the atmospheric radiative forcing is difficult because the positive greenhouses gases warming is perturbed by the presence of atmospheric particles [2,3], by the low accuracy of the greenhouse gases concentration spatial distribution and evolution and also by unknown physical and chemical processes. The above discussion is further described in the physical science basis IPCC report [1]. Moreover, in the long term, the Earth's climate is affected by the energy accumulation in the oceans, continents, and this on a time scale of several centuries whereby the atmospheric contribution is relatively small due to its low heat capacity. However, atmospheric greenhouse radiative forcing is still the long-lasting active contributor to the climate change.

Observation, modelling and analysis of the greenhouse gas concentration in the atmosphere is therefore an important task that helps to improve our knowledge on the climate trend and to organize realistic strategies and related actions to mitigate climate change. This is surely relevant for CH_4, the second supplier to the atmosphere radiative forcing after CO_2. Due to its relatively short lifetime (9 years) and its stronger warming efficiency than CO_2 (25×), reducing CH_4 emission could be an effective pathway to

* Corresponding author at: Institut Lumière Matière, CNRS, UMR 5306, Université Lyon 1, 10 rue Ada Byron, 69622 Villeurbanne, France.
E-mail address: patrick.rairoux@univ-lyon1.fr (P. Rairoux).

https://doi.org/10.1016/j.jms.2018.02.001
0022-2852/

reduce the impact of human activity on the Earth's climate at shorter timescales rather than only acting on CO_2 [4]. Today, the global mean CH_4 concentration in the atmosphere has a value of 1850 ± 3 ppb, which is known from the analysis of marine surface long-term observation [5]. Marine surface is there chosen because CH_4 sink is mainly achieved over land. However, the different CH_4 emission sources are subject to a high uncertainty: from 30% for anthropogenic emissions (agriculture, waste, fossils fuels use) up to 100% or more for natural sources (inlands water and geological) [6].

Following the previous remarks, methane in the Earth's atmosphere shows a growing interest in the scientific and socio-economical communities because its natural and anthropogenic emissions increase since a decade after a previous decade of constant concentration [7]. During the last decade, only positive concentration changes have been recorded with the extreme value of 12.59 ppb/year in 2014 [5]. The explanation of this increase is still uncertain but likely due in large parts to increases in fossil fuel consumption and biogenic emissions from agriculture and wetlands [6].

The reduction of these uncertainties requires to access local and regional emission fluxes which demand the development of new instruments and methodologies upon improving top-down and bottom-up models [4]. It is however not straightforward. Recent works showed interesting improvements to access field CH_4 flux measurements from ground-based instruments [8–13], air-borne lidar devices [14,15] and satellite-based remote sensing instruments like the future French-German MERLIN mission [16] to quote a few references. In these developments, optics plays a crucial role with emphasis on absorption spectroscopy and on CH_4 molecular spectroscopy in the NIR and IR spectral ranges. A review on in-situ optical instrumentation development for atmospheric trace gas detection can be found in Hodgkinson et al. [17]. CH_4 remote sensing applying Lambert-Beer law is mainly performed in the NIR $2\nu_3$ absorption band providing an optimum between light absorbance and detector efficiency [16,18]. Line strengths and line broadenings spectroscopy databases [19–21] are here necessary to achieve accurate light absorption measurements with a high spectral resolution.

In a recent contribution [22], we reported a laboratory work performed at the Institute of Light and Matter (ILM) in Lyon (France) showing broadband laser light absorption experiments in the CH_4 $2\nu_3$ band, by applying Optical Similitude Absorption Spectroscopy (OSAS). OSAS is based on the combined use of a broadband laser emission with an amplitude modulation spectrum. The concentration of the molecule of interest (i.e. the methane gas for example) is retrieved from a spectrally integrated differential absorption scheme using light sources having a spectral width that overlap several CH_4 absorption lines. This novel measurement method makes it possible to quantitatively retrieve a gas concentration from spectrally integrated absorption spectroscopy without the need for a concentration calibration procedure like as in standard spectrally integrated absorption spectroscopy [22]. This improvement has been made possible by the development of a novel mathematical formalism and a numerical algorithm to invert the Lambert-Beer-Bouguer's law. Hence, OSAS is a robust methodology for gas concentration measurement with a detection limit in the range of 1 000 ppm m for CH_4 [22]. OSAS is therefore a suitable methodology to evaluate gaseous emission. Moreover, we could show that the retrieved CH_4 concentration is not perturbed by atmospheric temperature and pressure conditions [23].

This paper reports on the first OSAS-Lidar experiment dedicated to CH_4 emission remote sensing directly into the atmosphere. A field experiment has been carried out using a controlled CH_4 emission source with concentration ranging from 15,000 ppm to few tens of ppb. The comparison with a standard analyzer measurement is achieved simultaneously. We show that, by applying the OSAS Lidar methodology, the observation of the rapid change of methane concentration is possible with a 1 s time resolution and with a statistical uncertainty of ±250 ppm. These specifications encounter estimated values presented in a previous work [18] and partially meet standard for hazardous emissions survey. This work was also dedicated to the study of concentration evaluation bias linked to the light source stability. We show that the light spectral density in terms of central wavelength and spectral width stabilities affects the sensitivity. Finally, we present for the first time the gas concentration-retrieval algorithm of OSAS-Lidar absorption measurements. This algorithm allows retrieving range-resolved and path-integrated concentrations. Due to the too low signal-to-noise ratio (SNR) of our OSAS-lidar signals, only path-integrated concentrations are here presented.

The paper is organized as follows. The OSAS-lidar principle is presented in Section 2 and the experimental implementation used to retrieve the methane concentration from the OSAS-lidar signals is presented in Section 3. Then, in Section 4, atmospheric OSAS-Lidar measurements are performed in the $2\nu_3$ CH_4 absorption band at the 1665 nm wavelength and compared with in-situ standard measurements. The paper ends with a conclusion and proposes outlooks on the OSAS-lidar CH_4 emission rate and emission flux remote sensing.

2. OSAS-Lidar principle

OSAS-Lidar is a spectrally integrated differential absorption lidar experiment where the laser emission spectral width is larger than the absorption line width of the absorbing molecules. Due to these spectral features, retrieving the concentration from the inversion of the light absorbance described by the Lambert-Beer-Bouguer's law is not straightforward. The methodology can be described by the following protocol: the atmosphere, containing the gas of interest, is excited with a reference then active pulsed broadband laser radiation. The reference light pulse is non-resonant with the absorption lines of the molecule of interest while the active light pulse is resonant with one or several absorption lines. After interrogating the time dependent laser light backscattering from the atmosphere, we retrieved the columned averaged of the target gas concentration from the active and reference spectrally integrated absorption signals. The retrieval procedure relies on specific experimental characterizations such as the input light power spectral density (PSD) and the detector optical response.

More formally, two different active and reference PSDs, $P_{0,1}(\lambda)$ and $P_{0,2}(\lambda)$ respectively, are generated. $P_{0,1}(\lambda)$ is set to match the 2 υ_3 absorption band of methane and $P_{0,2}(\lambda)$ is slightly off resonance with this band and serves a reference signal. The atmospheric backscattered signals $P_1(z)$ and $P_2(z)$ are collected with a telescope and correspond to the range-resolved output OSAS-lidar. The OSAS-Lidar formalism starts with the single scattering elastic lidar equation:

$$P_i(z) = \frac{K}{z^2}\int_{\Delta\lambda} O(z,\lambda)P_{0,i}(\lambda)\beta(\lambda)T_{TG}^2(z,\lambda)T_{atm}^2(z,\lambda)\eta(\lambda)\mathrm{d}\lambda \quad (1)$$

where K, is the opto-electronic constant, $O(z,\lambda)$ the overlap function, $\eta(\lambda)$ the detector efficiency (see Fig. 3) and $\beta(z,\lambda)$ the total backscattering coefficient at range z and wavelength λ. T_{atm} is the total transmission of the atmosphere, excluding the target-gas transmission. It includes absorption and scattering by molecules and particles. $T_{TG}(z,\lambda)$ is the transmission of the atmosphere only depleted by the absorption of target gas molecules:

$$T_{TG}(z,\lambda) = \exp(-2\sigma(\lambda)\int_0^z N_{TG}(z')dz') \quad (2)$$

where $\sigma(\lambda)$ is the absorption cross section of the target gas, $N_{TG}(z')$ is the target gas concentration expressed in molecules number per unit volume. We introduce $CC(z) = \int_0^z N_{TG}(z')dz'$, the cumulative concentration of the target gas as a function of the distance z.

To retrieve the target gas cumulative concentration $CC(z)$, the ratio $P_1(z)/P_2(z)$ is calculated and we verify that the overlap function $O(z)$ is the same over the mid-IR wavelength interval $\Delta\lambda$. The error on the retrieved target gas cumulative concentration induced by the wavelength dependence of the extinction and backscattering coefficients of the molecules and aerosols is negligible compared with our detector integrated concentration uncertainty of 250 ppm. As a matter of comparison, the same assumptions are satisfied for mid-IR DIAL experiment. The difference in the atmospheric extinction at the two spectral ranges relies solely on the target gas concentration. The contribution of the most important interfering gas, water, appears indeed negligible for methane concentration above 100 ppm [24].

To handle spectrally integrated absorption signals, the current approaches use the weak optical depths approximation [25]. In this framework, an effective absorption coefficient is introduced to mimic the overlap between molecular cross-sections and the PSD of the source. The latter must be linearized to allow the $CC(z)$ retrieval. Similarly, optical correlation spectroscopy (OCS) experiment takes advantage of a linear development of T_{atm} to retrieve the target gas concentration [18]. The OSAS methodology, free from the weak absorption approximation, offers a new approach that can address a variety of optical depths that follow Lambert-Beer-Bouguer law. Hence, we introduce an auxiliary function $f_i(z,x)$ which depends on the unknown target gas cumulative concentration x at a distance z from the laser emission position.

$$f_i(z,x) = \int_{\Delta\lambda} P_{0,i}(\lambda)\exp[-2\sigma_{TG}(\lambda)x(z)]\eta(\lambda)\mathrm{d}\lambda \tag{3}$$

The ratio $f_1(z,x)/f_2(z,x)$ should have the same numerical value as the ratio $P_1(z)/P_2(z)$ for x equal to $CC(z)$. We are therefore looking for the first zero of the function $g(z,x)$ defined by:

$$g(z,x) = P_2(z)f_1(z,x) - P_1(z)f_2(z,x) \tag{4}$$

Numerous root-finding methods can be used to retrieve the concentration N. We use the popular secant root-finding algorithm for its fast convergence. The convergence of the algorithm is guaranteed if a change in the target gas cumulative concentration induces a change in the ratio $f_1(z,x)/f_2(z,x)$ with always the same trend. This monotonic behavior is ensured for the whole range of optical depths present in Earth atmospheric conditions.

To highlight the convergence of the inversion algorithm in the case of a high methane optical depth, typical g -function for different P_1/P_2 signals ratio are displayed in Fig. 1.

To extract the range-resolved concentration, we apply the root-finding algorithm on the g-function at each range $[0,z]$. A cumulated concentration $CC(z)$ is therefore obtained. The target gas concentration N_{TG} at range z is retrieved by computing the derivative of $CC(z)$ with respect to z:

$$N_{TG}\left(z+\frac{\Delta z}{2}\right) = \frac{dCC(z)}{dz} \tag{5}$$

where Δz is the spatial resolution.

3. Experimental setup

The CH_4 OSAS-Lidar experiment is schemed in Fig. 2. We will start the description with the optical parts of the system, before explaining the spectral calibration procedure. This latter is necessary to retrieve a quantitative concentration value from measurements following OSAS methodology. This section ends with the measurement strategy applied to compare OSAS-Lidar with in-situ point measurements achieved with a standard device.

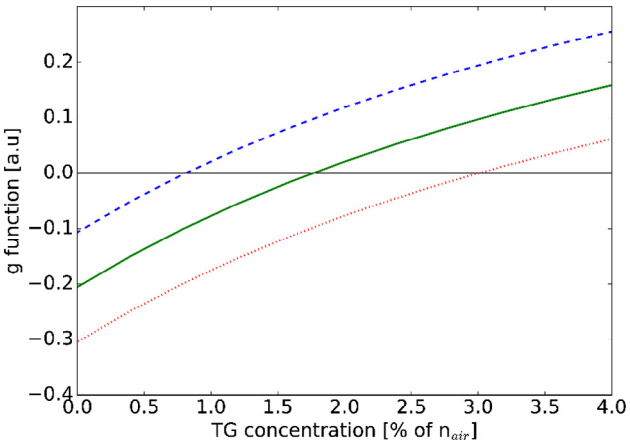

Fig. 1. g functions for three different P_1/P_2 signals ratio. The target gas cumulative concentration corresponds to the first root of the g function. Blue stray line: $P_1/P_2 = 0.95$, $N = 0.81\%$; green plain line: $P_1/P_2 = 0.9$, N = 1.76% and red dotted line: $P_1/P_2 = 0.85$, $N = 3.00\%$.

A Ti:Sa laser (30 MHz repetition rate, 1nJ pulses, 100 fs pulse duration) is amplified in a two amplification stages process: a regenerate amplifier and a multi-pass amplifier. This commercial amplifier system (Integra HE Quantronix®) generates 4 mJ pulses centered at 780 nm at 1 kHz repetition rate. This radiation seeds a commercial optical-parametric-amplifier (Quantronix®) to generate 600 μJ idler pulses at 1660 nm. The idler and signal pulses are separated thanks to their different state of polarization. Two portions of the total spectrum of the idler pulse must be selected to create the active and reference channel ($P_{0,1}(\lambda)$ and $P_{0,2}(\lambda)$). An acousto-optic programmable dispersive filter (AOPDF) from Dazzler company performed this selection. The AOPDF, triggered with the 1 kHz synchronization signal of the amplified pulses, selects successively the narrower spectra $P_{0,1}(\lambda)$ and $P_{0,2}(\lambda)$. The spectral switch between the active and reference channel operates at 100% duty cycle. The selected spectra are shown in Fig. 3.

The PSDs measurement is performed using an IR Czerny-Turner type spectrometer by Andor® with a spectral resolution of 0.1 nm around 1660 nm. The width of the AOPDF spectral selection has been set to 2.28(3) nm, which corresponds to the minimum achievable width of the AOPDF. This spectral width ensures a high pulse energy leading to a sufficient concentration sensitivity on CH_4 emission. The maximum energy obtained after the spectral selection is approximately 30 μJ, just below the theoretical AOPDF input limit. Stability measurements performed on the laser spectra modulated by the AOPDF indicate a spectral width standard deviation of 0.03 nm over 15 min of acquisition (see Fig. 4). The center wavelength of the selected spectra is stable within 0.05 nm and the spectra area have fluctuated by less than 10% during this time slop.

Before performing OSAS-lidar measurements, prior spectral characterizations are necessary as mentioned earlier. Fig. 3 summarizes the spectral data used in the retrieval algorithm. The methane cross-section is calculated from the HITRAN-database with standard pressure and temperature. To measure the efficiency $\eta(\lambda)$ of the APD, the central wavelength filtered by the AOPDF is swept from 1600 to 1710 nm by steps of 1 nm. One part of the filtered light is analyzed with the spectrometer. Another part propagates through a 1 m optical gas cell filled with 1 atm of pure N_2. Hence, the APD efficiency is evaluated from the simultaneous measurement of the incoming radiation PSD and the signal amplitude on the APD detector. To validate our spectral calibration, we performed in laboratory a methane path integrated concentration

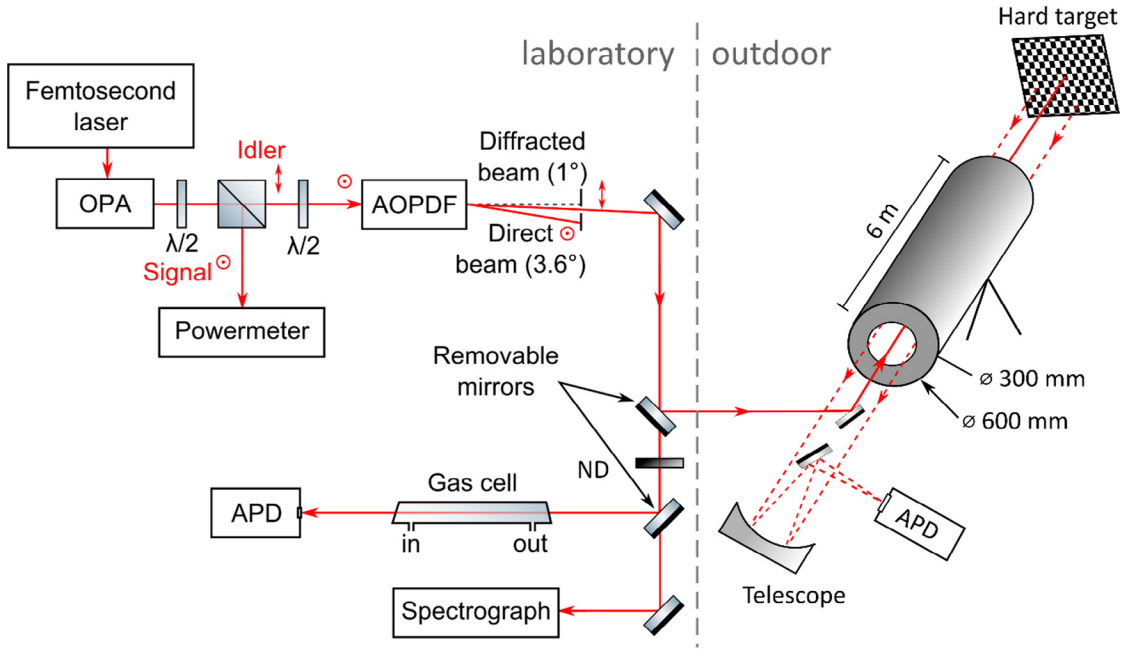

Fig. 2. The OSAS-Lidar experimental implementation. The IR light pulses, generated by an Oscillator Parametric Amplifier (OPA) are spectrally modulated using an Acousto-Optic Programmable Dispersive filter (AOPDF). Spectral calibrations of the light pulses PSD and the efficiency of the Avalanche Photodiode (APD) are performed in laboratory. The gas cell in the laboratory enables laboratory tests. The outdoor OSAS-Lidar experiment is carried out by sending the light pulses outside the laboratory, through a 6 m long pipe used as CH_4 emitter proxy.

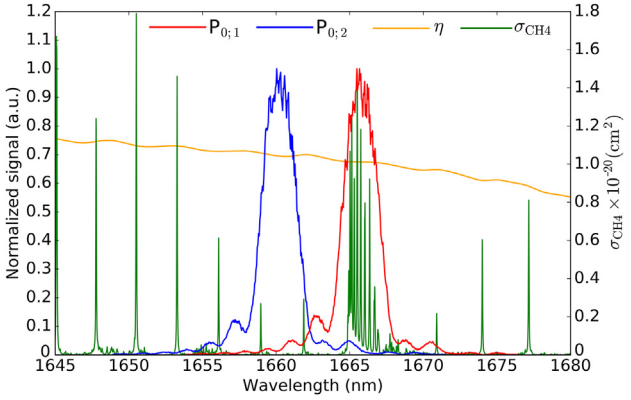

Fig. 3. Spectral characterization for the OSAS inversion. The power spectral density of the active channel (red curve) and the reference channel (blue curve). The methane absorption cross-section spectrum $\sigma_{CH4}(\lambda)$ of the $2\nu_3$ absorption band is here considered (green lines), calculated from HITRAN 2012 database [21] for T = 294 K, p = 1013.25 mbar and air-broadening; a Voigt profile is used to model the line-shape. $\eta(\lambda)$ is the spectrum of the opto-electronic efficiency of the OSAS detection part (orange curve).The power spectral density of $P_{0,1}(\lambda)$ and $P_{0,2}(\lambda)$ must be carefully measured to ensure a reliable gas concentration retrieval procedure.

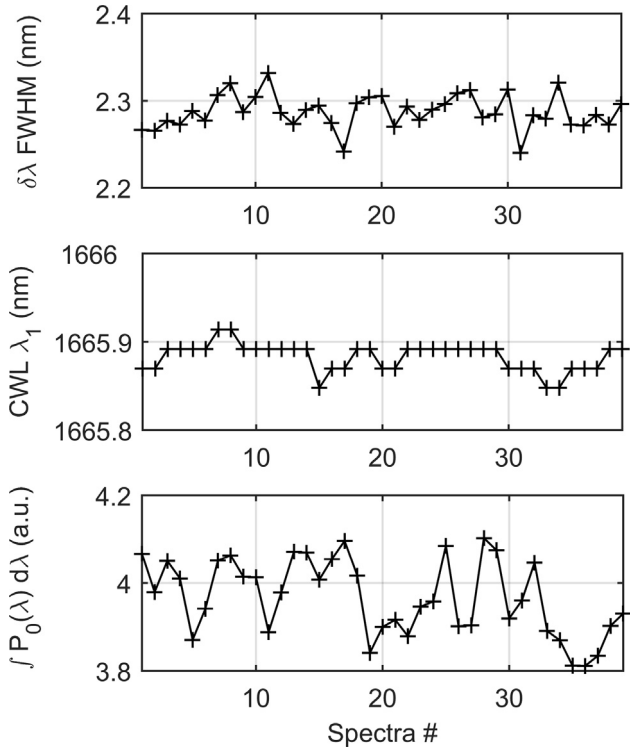

Fig. 4. Spectral width at FWHM, central wavelength and frequency-integrated value of the laser spectral power density as a function of each individual 39 recorded spectrum. The spectrum are recorder in a laps time of 15 min.

(PIC) measurement by filling the 1 m optical gas cell with a mixture of 4% methane, 96% N_2. As shown in Fig. 5, we successfully retrieve the methane PIC using the OSAS methodology and our spectral calibrations.

From the PSD stability measurement (see Fig. 4), we evaluate that the systematic error due to PSD fluctuations accounts for less than 2% for 10^4 ppm m of methane.

To carry out OSAS-Lidar in the atmosphere we use a standard lidar device set-up. As the amplitude modulation is performed at the emission, the lidar receiver configuration is quite simple. The backscattered radiation is collected with a Newtonian telescope of 450 mm focal length with a primary mirror of 115 mm diameter. The detection consists in a single APD photo-detector mounted at the telescope focus point. The two OSAS-lidar signals $P_1(z)$ and $P_2(z)$ are successively recorded with a 12-bit resolution oscilloscope at a 1 kHz repetition rate.

To demonstrate OSAS-lidar methodology as a remote-sensing system of gaseous emission in the atmosphere, a proxy of a

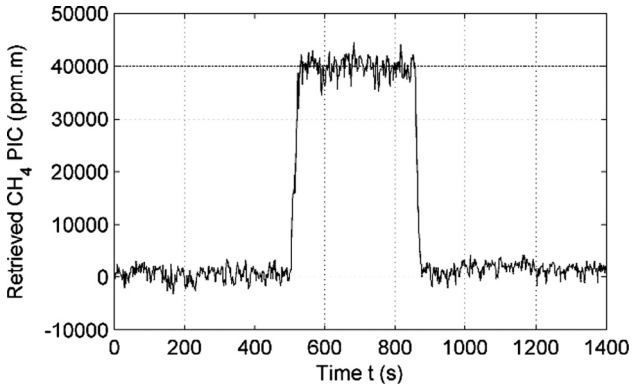

Fig. 5. Temporal evolution of methane path integrated concentration (PIC) measured in laboratory for spectral calibration verification. At time t = 500 s, the 1-meter-long laboratory gas cell buffered with N_2 is filled with a methane-air mixture (4% of methane). Then, methane is removed from the gas cell by flushing it with N_2.

low-pressure methane leak is created by filling the pipe with 1.5% of methane as depicted in Fig. 2. The pipe diameter is 0.6 m and the diameter of its endpoints is twice smaller to slow down the methane gas outflow once the end-caps are removed. The filling process is performed at atmospheric pressure by partially closing both ends.

The IR laser radiation is sent horizontally into the atmosphere and crosses the pipe at its center before being reflected by a hard target located ~110 m away from the lidar detector.

During the OSAS-Lidar experiment, we simultaneously measure the gas concentration in the pipe with a local analyzer (a flam ionization detector (TVA-1000 from the Foxboro company provided by CleanAir®), placed at 5 cm from the pipe wall.

This configuration minimizes straight light from the in-situ measurement device illuminated by the laser beam that can interfere the OSAS-Lidar experiment. On the other hand, this configuration leads to difference on the sampled volume as depicted Fig. 6. Within this configuration, once the proxy leak is filled with CH_4 and the pipe caps are removed the pipe is progressively replaced with fresh air. As methane releases the pipe, it immediately disperses into the atmosphere. Therefore, methane is considered only in the pipe and the effective methane light absorption path decreases with time (see Fig. 6a). Contrariwise, the local analyzer probes the same small volume at the vicinity of its probe. As a result, the cumulative gas concentration measured by OSAS-lidar first decreases linearly as the pipe empties while the local analyzers measure a steady methane concentration (a laminar flow hypothesis is there considered). Once fresh air has reached the volume probed by the analyzer, the methane concentration measured by the local analyzer will decrease rapidly. OSAS-lidar cumulative concentration is normalized by the length of the pipe to compare both measurements, and it allows a proper comparison at the measurement starting point (see Fig. 6(b)).

4. Results

We here first present range-resolved OSAS-lidar signals obtained from the IR laser light backscattering from the atmosphere. These measurements enable to evaluate the range-resolved signal to noise ratio (SNR) level in absence of CH_4. Second, we present for the first time CH_4 emission monitoring using OSAS-lidar from a proxy source and discuss the comparison with the in-situ analyzer.

The time-resolved measurements of the laser radiation backscattered from the atmosphere (see equation1) and from the hard target are achieved with a 500 MHz bandwidth acquisition system. Considering back and forth light propagation, it corresponds to a 3 m range resolution when applying a 10 points binning to the detected backscattered signal. For the target backscattered signal, the full bandwidth is considered, allowing a higher spatial resolution. In the absence of CH_4, OSAS-lidar signals from the 30 μJ laser pulses $P_{0,1}(\lambda)$ et $P_{0,2}(\lambda)$ operating at 1665.5 nm and 1660 nm respectively are presented in Fig. 7 (top). The objective here is to evaluate the range-resolved SNR of the lidar signals. Each curves shown in Fig. 7 is a 2.5 min time-averaged of single lidar signals with a range resolution of 3 m. The backscattering lidar signal shows a maximum at 50 m and then decreases following the change of the receiver solid angle with distance ($1/z^2$). The signal is maximal at z = 50 m, as a result of the optimization of the lidar overlap function, the latter being constant from 50 m to the hard target position. From 0 to 20 m, stray lights are visible due to scattering on the laser beam guiding mirrors. Fig. 7 (bottom) shows the corresponding $P_1(z)/P_2(z)$ ratio. Due to the low backscattered light power, CH_4 concentration retrieval applying OSAS methodology on the atmosphere-backscattered signals is found to be too noisy. This is mainly due to the limited sensitivity on the $P_1(z)/P_2(z)$ ratio (see Fig. 7 bottom between 0 and 108 m). However, the SNR on the hard target backscattered signal is larger (SNR = 103 compared to SNR = 2 at z = 50 m on the atmosphere backscattered signal). As shown in Fig. 7 (bottom), the sensitivity on the ratio is 6 times better at the range of 108 m using the backscattered signals from the hard target. We therefore perform the OSAS-methodology on the signals backscattered by the hard

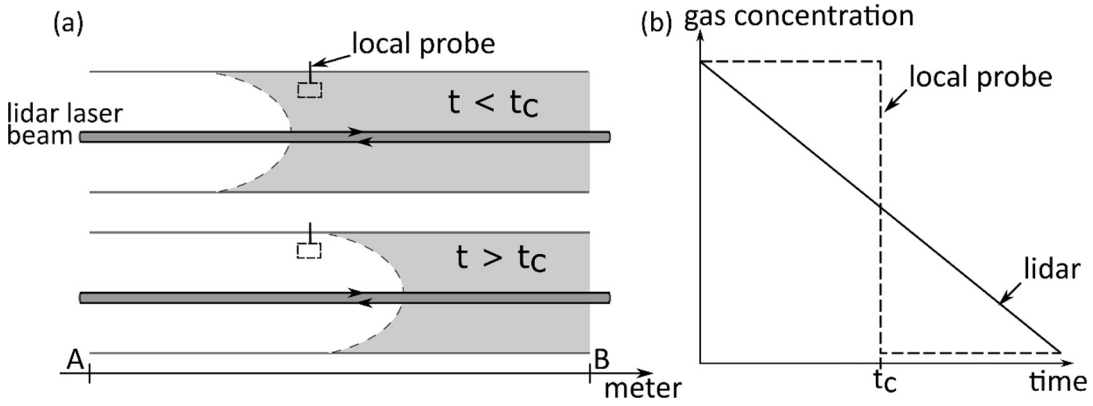

Fig. 6. Coarse simulation of the evolution of the retrieved methane concentration for the local analyzer and the OSAS-lidar experiment, considering a fixed absorption length AB. (a) the wind pushes the methane enhanced gas (gray area) from A point to B point towards open air. (b) The signals of the two sensors, proportional to the retrieved methane concentration, show different temporal behaviors (see text).

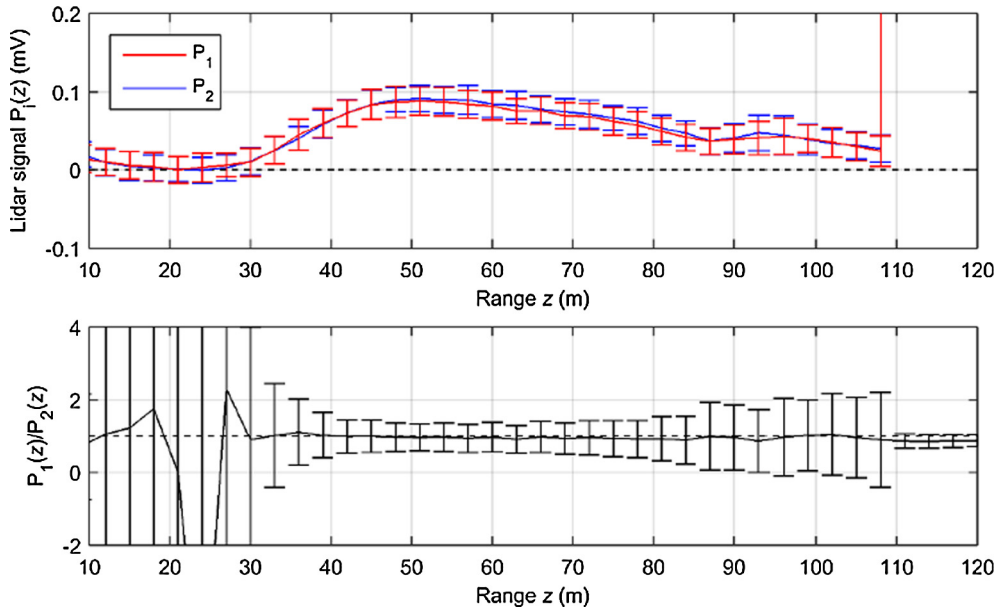

Fig. 7. Top: Range resolved backscattering signal (background corrected) from the atmosphere (molecular and aerosol contribution) and hard target in the absence of CH_4 emission for the active channel at 1665.5 nm (red) and the reference channel at 1650 nm (blue). The strong signal increase at the range z = 108 m is the signature of the hard target laser light backscattering. Scaling of the y-axis is adjusted to highlight the signal backscattered by the atmosphere only. Bottom: ratio of both lidar signals. The dashed line is set at $P_1/P_2 = 1$. The errors bars are calculated from the standard deviation of the 360 lidar signals individually averaged over one second.

target $P_i(z = 108\ \text{m})$ to evaluate the cumulative methane concentration $CC(z = 108\ \text{m})$, referred to as path-integrated concentration (PIC) in what follows. Because lidar measurements rely now on hard target returns, only PIC retrievals can be considered. Moreover, Fig. 7 (top) shows that the lidar signals ratio $(P_1(z)/P_2(z))$ remains constant over the considered range within error bars. This clearly indicates that the lidar receiver observes both laser beams (the reference and the active one) within the same field of view, which is a prerequisite in differential absorption lidar methodology, to avoid concentration biases.

Simultaneous OSAS-Lidar and in-situ measurements of CH_4 concentration evolution from the proxy emitter flow-out are shown in Fig. 8. The OSAS Lidar retrieved concentrations (black curve) are path-integrated concentrations normalized by the 6 m long methane emission pipe. The removal of the pipe end-caps marks the temporal starting point of the OSAS-lidar signals acquisition. The concentration values from both measurement devices show different time behavior. After the pipe has been filled to a constant concentration of 15000 ppm, the in-situ analyzer shows for several minutes a constant value that decreases rapidly to lower value (3000 ppm). During this time interval, the OSAS-Lidar CH_4 concentration values decrease rapidly from the start concentration value (within the error bars) to 5000 ppm. This rapid decrease is related to the presence of a breeze at the beginning of the experiment that increases CH_4-release rate from the pipe. The start of the concentration decrease shows a two minutes delay between the two measurements than can be explained from the local probing and lidar sensing geometry, as explained in Section 2. Later (at 22:05), the breeze slows down and consequently the OSAS-Lidar measurements show a linear decrease (within error bars) related to a slower CH_4 pipe empting. This behavior can also be related to the CH_4 sensing geometry (see Section 2). Therefore, both devices show different concentration values apart from the beginning of the measurement. At 22:08, the methane concentration briefly remained constant as the breeze stopped. At 22:12, a second breeze ended up to empty the pipe. Due to the inherent turbulent behavior of the atmosphere, our explanation remains however approximate. To improve the analysis of this measurement comparison, a precise knowledge of the wind field is necessary. Nevertheless, the OSAS-lidar and local analyzer measurements agree within the error bars (±250 ppm) at the very first measurement points.

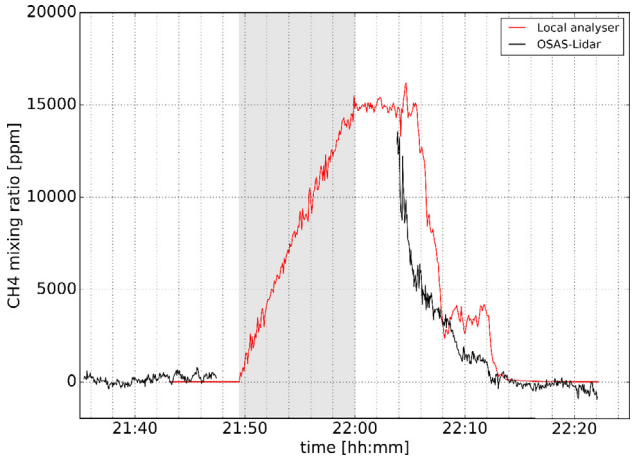

Fig. 8. Methane measurements on a CH_4 outdoor proxy source emission performed at Lyon on October 7, 2017 with OSAS-Lidar (black) and standard point measurement analyzer (red). Measurement accuracy of OSAS-lidar and in-situ analyzer is 2000 ppm m and 1% respectively. For sake of clarity error bars are not drawn. The gas cell is closed and filled with methane during 16 min (time slot indicated by the grey area). CH_4 mixing ratio measured with OSAS-Lidar and the standard analyzer behave differently because the probed volumes are not the same as depicted in part 2.

5. Conclusion

In this paper, a methane emission remote sensing experiment has been carried out directly in the atmosphere by using a new lidar device, called the OSAS-lidar device, and compared with a local standard analyzer. We could hence proof that the OSAS-lidar methodology, based on the inversion of the spectrally integrated absorption Lambert-Beer-Bouguer law, is suitable for trace

gas remote sensing and this without considering the low absorbance assumption and without gas concentration calibration procedure. As a counterpart, this new methodology demands a precise spectral calibration of the detector and of the laser power spectral density, but the latter can be performed directly in a controlled-laboratory experiment.

The use of broadband laser emission in regards to the spectral width of the absorbing species renders the absorbance contrast low, which directly influences the measurement sensitivity. This characteristic makes the application of OSAS-Lidar more appropriate to the detection of high gas concentration releases into the atmosphere. There, the quasi-non dependence of OSAS measurement to atmospheric temperature and pressure conditions is a subsequent benefit. Moreover, monitoring gaseous releases demands a measurement ability with a fast response time. The here presented new OSAS-Lidar device successfully meets this requirement (1 s time resolution).

We could also observe that the accuracy of the OSAS-lidar measurement (±250 ppm) is affected on one hand by the low SNR of the InSb detector used in the experiment and on the other hand by the laser emission jitter in terms of PSD stability as explained in Section 2. Finally, the OSAS-lidar sensitivity is one order of magnitude lower than the high spectral resolution DIAL [26].

Molecular spectroscopy data does not influence the accuracy of the OSAS-Lidar measurement in regards to its sensitivity. Recent improvements in the CH_4 spectroscopy parameters database could have a strong contribution to the improvement of OSAS bias reduction by minimizing the error linked to absorption cross-sections in the $2\nu_3$ methane absorption band. Possible interferences and resultant biases induced by the presence of other trace gas species absorbing in the same spectral range as methane must be precisely evaluated. It is the case for water vapor whose absorption would perturb the measurement at CH_4 concentration lower than 100 ppm.

Outdoor comparison between different instruments still remain very challenging, as the meteorological conditions can never be considered as stable and as the instruments do not necessarily probe the same atmospheric volume. To better evaluate the systematic errors on the retrieved CH_4 concentration from OSAS-lidar, it is worth considering testing this new methodology with another methane lidar system (as DIAL) where the sensing volume can be similar. Another outlook will be the coupling CH_4 OSAS-Lidar with a wind lidar in order to access a direct measurement of time resolved CH_4 emissions flux on large areas that could be helpful in regard to climate change mitigation.

Acknowledgements

We thank Pr. Lionel Soulhac from LMFA Lyon for fruitful discussions on fluid dynamics.

References

[1] T.F. Stocker, D. Qin, G.K. Plattner, M. Tignor, S.K. Allen, J. Boschung, A. Nauels, Y. Xia, B. Bex, B.M. Midgley, IPCC, 2013: Climate Change 2013: The Physical Science Basis. Contribution of Working Group I to the Fifth Assessment Report of the Intergovernmental Panel on Climate Change, Cambridge University Press (Ed.) (2013).
[2] A. Miffre, C. Anselmo, G. David, G. Geffroy, E. Fréjafon, P. Rairoux, Opt. Express 23 (3) (2015) 2347–2460.
[3] M. Schulz et al., Atmos. Chem. Phys. 6 (2006) 5225–5246.
[4] M. Saunois, R.B. Jackson, P. Bousquet, B. Poulter, J.G. Canadell, Environ. Res. Lett. 11 (120207) (2016) 1–5.
[5] Ed. Dlugokencky, NOAA/ESRL, www.esrl.noaa.gov/gmd/ccgg/trends_ch4/.
[6] M. Saunois et al., Earth Syst. Sci. Data 8 (2016) 697–751.
[7] S. Kirschke et al., Nature Geoscience 6 (2013) 813–823.
[8] T. Gardiner, J. Helmore, F. Innocenti, Rod Robinson, Remote Sensing 9 (9) (2017) 956.
[9] F. Innocenti, R. Robinson, T. Gardiner, A. Finlayson, A. Connor, Remote Sensing 9 (9) (2017) 953.
[10] M.F. Hendrick, R. Ackley, B. Sanaie-Movahed, X. Tang, N.G. Phillips, Environ. Pollut. 213 (2016) 710–716.
[11] D. Fu, T.J. Pongetti, J.-F.L. Blavier, T.J. Crawford, K.S. Manatt, G.C. Toon, K.W. Wong, S.P. Sander, Atmos. Meas. Tech. 7 (2014) 713–729.
[12] G.B. Rieker, F.R. Giorgetta, W.C. Swann, J. Kofler, A.M. Zolot, L.C. Sinclair, E. Baumann, C. Cromer, G. Petron, C. Sweeney, P.P. Tans, I. Coddington, N.R. Newbury, Optica 1 (5) (2014) 290–298.
[13] A. Diaz, B. Thomas, P. Castillo, B. Gross, F. Moshary, Applied Physics B 122 (2016) 121.
[14] C. Weaver, C. Kiemle, S.R. Kawa, T. Aalto, J. Necki, M. Steinbacher, J. Arduini, F. Apadula, H. Berkhout, J. Hatakka, Atmos. Chem. Phys. 14 (2014) 2625–2637.
[15] A. Amediek, G. Ehret, A. Fix, M. Wirth, C. Büdenbender, M. Quatrevalet, C. Kiemle, C. Gerbig, App. Opt. 56 (2017) 5182–5197.
[16] G. Ehret et al., Appl. Phys. B 90 (2008) 593–608.
[17] J. Hodgkinson, R.P. Tatam, Meas. Sci. Technol. 24 (1) (2013). 012004 1-59.
[18] B. Thomas, A. Miffre, G. David, J.P. Cariou, P. Rairoux, Appl. Phys. B 108 (2012) 689–702.
[19] T. Chesnokova, V. Boudon, T. Gabard, K.G. Gribanov, K. Firsov, V.I. Zakharov, J. Quant. Spectrosc. Radiat. Transf. 112 (2011) 2676–2682.
[20] A. Campargue, O. Leshchishina, L. Wang, D. Mondelain, S. Kassi, J. Mol. Spectrosc. 291 (2013) 16–22.
[21] L.S. Rothman et al., J. Quant. Spectrosc. Radiat. Transf. 130 (2013) 4–50.
[22] C. Anselmo, J.-Y. Welschinger, J.P. Cariou, A. Miffre, P. Rairoux, Opt. Express 24 (12) (2016) 12588–12599.
[23] B. Thomas, A. Miffre, G. David, C. Anselmo, E. Coillet, J.P. Cariou, P. Rairoux, J. Mol. Spectrosc. 291 (2013) 3–8.
[24] B. Thomas, G. David, C. Anselmo, A. Miffre, J.P. Cariou, P. Rairoux, Appl. Phys. B 113 (2013) 265–275.
[25] C. Massie, G. Stewart, G. McGregor, J.R. Gilchrist, Sens. Actuat. B Chem. 113 (2) (2006) 830–836.
[26] J. Barrientos Barria et al., Appl. Phys. B 117 (2014) 509–518.